A Comparative Study Between the Nearest Three Vectors and Two-Level Hexagons Based Space Vector Modulation Algorithms for Three-Level NPC Inverters

Zouhaira Ben Mahmoud *‡, Mahmoud Hamouda *, and Adel Khedher *

* Research Laboratory LATIS, ENISO, University of Sousse, 4023, Tunisia

(benmahmoud_zouhaira@yahoo.fr, Mahmoudhamouda@yahoo.fr, adel_kheder@yahoo.fr)

‡ Zouhaira Ben Mahmoud, BP 264, Riadh City, 4023, Sousse, Tunisia

Received: 23.12.2016 Accepted:20.04.2017

Abstract- Multi-level power converters are nowadays the most appropriate solution for medium-voltage grid-connected Renewable Energy Sources (RES) such as variable speed wind-turbines and photovoltaic (PV) generators. Basically, there exist two space vector modulation (SVPWM) schemes which are commonly used to modulate the output voltages provided by three-level inverters. For the first method, namely the nearest three vectors (NTV), the position of the space vector is identified in one of the triangles forming the space vector diagram. As for the second method that is referred to as the hexagon technique, the opportune position of the space vector is determined within a two-level hexagon. This paper is therefore focused on a comprehensive comparative study between the performances of the two aforementioned techniques. The evaluation is performed in terms of Common Mode Voltages (CMV), Total Harmonic Distortion (THD), conducted emissions, and efficiency. The proposed comparison is based on numerical simulations and experimental tests. The obtained results confirm that the NTV technique provides the better performances in terms of THD and CMV for low modulation index values. It also provides less common mode emissions when the modulation index is near its maximum value. As for the efficiency, both methods provide the same performance for a modulation index superior or equal to 0.8.

Keywords Multi-level converters, neutral-point-clamped (NPC) inverter, common mode voltages (CMV), space-vector modulation (SVPWM), conducted emissions (EMI), total harmonic distortion (THD), efficiency.

1. Introduction

In nowadays, the interest in multi-level inverters has remarkably increased, mainly, due to the huge development in power electronics technology and to the massive use of high power medium-voltages equipment within the domain of the industry [1-3]. Indeed, they are the most suitable solution to be easily interfaced with renewable energy sources (RES) such as for example the photovoltaic systems and variable speed wind turbines [4-8]. They allow also the connection of the RES to the medium voltage grid without utilizing an expensive and bulky transformer. When compared with two-level inverters, multilevel topologies offer many significant advantages such as a reduced voltage stress on power semiconductors, less harmonic content in the output voltage waveforms, and a better efficiency [9, 10].

A variety of power conversion topologies has been proposed with the aim to improve the efficiency and reduce the control complexity. The most known are: flying-capacitors (FC) converter, cascaded H-bridge (CHB) inverter, packed U cells [11, 12] and neutral point clamped (NPC) inverter [13]. The NPC inverters represent nowadays one of the most popularly utilized topologies in the industrial field thanks to their higher performance compared to the FL inverters and the use of a unique DC source of voltage when compared with the CHB inverters [14, 15]. On the other hand, various modulation strategies were developed with the aim to allow the converter accurately synthesizing the desired voltage system. The most known techniques are: the Sinusoidal Pulse Width Modulation (SPWM) with and without harmonic injection [16-19], as well as the Space-Vector modulation (SVPWM) [20, 21]. Despite being one of the most complex methods to be implemented, the latter SVPWM offers more freedom when determining the switching sequences which reduces the switching losses and results in a balanced neutral point voltage and a lessened common mode voltage [22]. The SVPWM is basically classified into two categories: the Nearest Three Vectors (NTV) method and the Hexagons method. For the NTV approach, the output voltage-vector is modulated by making an appropriate combination of the nearest three vectors [23]. For this reason, the sector including the target output voltage vector is split into many triangles; the appropriate triangle containing the tip point of this latter is then identified. This method is very simple when applied to three-level

inverters, however, if the level's number increases ($n > 3$), the number of triangles and switching states increase as well, which makes its implementation much more complex [24]. For the hexagon's approach, the output voltage vector is synthesized using the similar manner as the conventional 2-level converter. The tip-point of the space vector is therefore identified inside a two-level hexagon also called small hexagon. The implementation of this technique is easier than the NTV approach. A variety of modulation techniques have been proposed to further simplify this method when n exceeds 3. In [25], a coordinate transformation was proposed to create the target output-voltage vector. In [26], the n-level space vector diagram is reduced to the 2-level space vector diagram by shifting the sub hexagon including the reference voltage vector towards the inner sub-hexagon. In [27,28], the five-level vector diagram is simplified in a first step into a three-level diagram; in the second step it is reduced to a simple two-level hexagon. In [24], a fast and simple approach was proposed. The latter consists in directly reducing the n-level diagram to the 2-level one enclosing the space vector.

On the other hand, the performance of PWM modulation schemes can be assessed in terms of power-semiconductors switching losses, the modulated output voltages, Total Harmonic Distortion (THD), the Common Mode Voltage (CMV) that is the electric potential of the load neutral point refereed to the ground [29], conducted emissions, efficiency, etc. Unfortunately, the existing literature lacks deep research works focusing on such comparative studies between the performances of modulation schemes for multilevel inverters. In this context, this works is carried out in order to perform a comprehensive comparison concerning the two most popular SVPWM techniques for three-level inverters: the NTV and two-level hexagon (small hexagon) methods. This study is realized in terms of the aforementioned performance criteria for wide range of the modulation index.

To achieve these goals, this paper will be decomposed into six sections. A brief review of the 3-level NPC converter and its space vector diagram are provided in section 2. Sections 3 and 4 explain respectively the theories of NTV and two-level hexagon methods. The numerical and experimental tests will be performed successively in section 5 and 6. Finally, a general conclusion is provided at the end of this paper.

2. Three-phase Three-level NPC Converter Topology

NPC inverters represent nowadays one of the most popular and commonly used topologies in the industrial areas since they have the benefit of low current THD and having a split dc capacitors structure that leads to a decreasing voltage stress and, thereby, reduces the electromagnetic interference (EMI) [30]. In general, a three-phase n-level NPC inverter contains three legs; each one is built with $2\,(n-1)$ power transistors with their free-wheeling diodes and $2(n-2)$ clamping diodes [31]. $(n-1)$ capacitors are connected in series across the dc-bus so as to obtain $(n-1)$ floating dc potentials. The three-level NPC inverter, given by Fig. 1, consists therefore of 4 power transistors with 4 free-wheeling diodes and 2 clamping diodes for each leg. Its two dc terminals are connected to a dc voltage source V_{dc}. The latter is split into two floating potentials successively named V_{Po} and V_{No} due to the use of two similar series connected capacitors. The converter's poles (a, b, c) are linked to a three-phase load operating as a current source. Basically, each leg has three switching states defined as follows [32]:

- State P: the two upper switches are ON state. The modulated voltage $V_{xo\ (x=a,b,c)}$ is therefore equal to $V_{dc}/2$.

State O: the two middle switches are ON state. The modulated voltage $V_{xo\ (x=a,b,c)}$ is equal to 0.

State N: the two lower switches are ON state. The modulated voltage $V_{xo\ (x=a,b,c)}$ is equal to $-V_{dc}/2$.

Consequently, the total number of the converter's switching states is equal to $3^3 = 27$ giving rise to 27 space vectors as represented in Fig. 2. These vectors are arranged into four categories:

Three *zero vectors* denoted V_0.

Six *small vectors* namely V_1- V_6; their amplitude is equal to $V_{dc}/3$.

Six *medium vectors* namely V_8, V_{10}, V_{12}, V_{14}, V_{16}, V_{18}; their amplitude is equal to $V_{dc}/\sqrt{3}$.

Six *large vectors* namely V_7, V_9, V_{11}, V_{13}, V_{15}, V_{17}; their amplitude is equal to $2V_{dc}/3$.

The SVPWM based control technique determines a complex reference vector $\overline{V_r}$ equivalent to the target three-phase output voltages. The position of this vector is usually determined in a two-phase reference frame. Therefore, at each sampling time, we should determine the appropriate adjacent space vectors as well as their duty ratios allowing the synthesis of $\overline{V_r}$ in an average sense. Two popular modulation methods have been widely used in the recent literature to modulate $\overline{V_r}$ namely, the Nearest Three Vectors (NTV) and the Hexagon methods. For a better understanding of this paper, their theoretical principles are briefly reviewed in sections three and four hereafter.

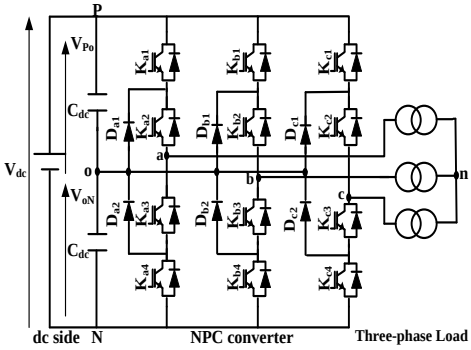

Fig. 1. Schematic circuit of three-level NPC inverter

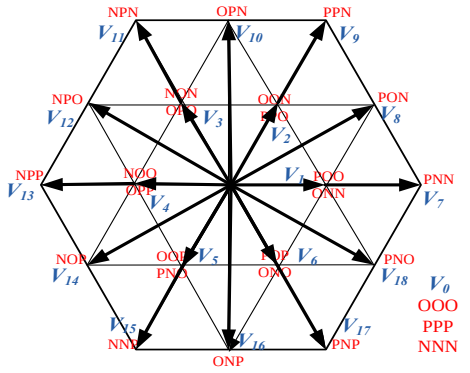

Fig. 2. Space-vector diagram of 3-level NPC converter

3. The NTV Method

Basically, the vector diagram of the inverter is divided into six sectors ($k_v = 1,2,..,6$). Each sector is made up of $(n-1)^2$ triangles or regions, where n is the levels' number. For the three-level inverter, one can have only four triangles in each

sector. Then, the SVPWM scheme can be easily implemented considering three main steps: three nearest vectors identification or triangle identification, duty cycles computation, and switching sequences generation.

Firstly, we define the reference-vector coordinates $\overline{V}_r$ in the (α,β) stationary-frame using the conventional Clark transformation shown in Eq. (1):

$$\begin{bmatrix} V_{\alpha\_r} \\ V_{\beta\_r} \end{bmatrix} = \frac{2}{3} \begin{bmatrix} 1 & -\frac{1}{2} & -\frac{1}{2} \\ 0 & \frac{\sqrt{3}}{2} & -\frac{\sqrt{3}}{2} \end{bmatrix} \begin{bmatrix} V_a \\ V_b \\ V_c \end{bmatrix} \quad (1)$$

With V_a,V_b and V_c are the target output voltages.

This vector ($\overline{V}_r = V_{\alpha_r} + jV_{\beta_r}$) can be located in one of the four triangles as shown in Fig. 3. To identify the appropriate triangle number, we shall firstly determine the generalized reference-vector coordinates V'_α and V'_β , as reported in Eq(2.a) [26]:

$$\begin{cases} V'_\alpha = |\overline{V}_r| \cos\left(\theta - (k_v - 1)\frac{\pi}{3}\right) \\ V'_\beta = |\overline{V}_r| \sin\left(\theta - (k_v - 1)\frac{\pi}{3}\right) \end{cases} \quad (2.a)$$

With, θ and k_v are the instantaneous phase angle and operation sector of the reference vector $\overline{V}_r$.

The appropriate triangle (region) that contains the reference-vector is then identified according to a specific algorithm as depicted in Eq. (2.b) [26]:

$$\begin{cases} \text{if} \quad V'_\alpha < \frac{V_{dc}}{3} - \frac{\sqrt{3}}{3}.V'_\beta & \text{then triangle} = 1 \\ \text{Else if} \quad V'_\alpha > \frac{V_{dc}}{3} + \frac{\sqrt{3}}{3}.V'_\beta & \text{then triangle} = 4 \\ \text{Else if} \quad V'_\beta < \frac{\sqrt{3}}{6}.V_{dc} & \text{then triangle} = 2 \\ \text{Else} & \text{triangle} = 3 \end{cases} \quad (2.b)$$

With, V_{dc} is dc-bus voltage.

Once the triangle is identified, the reference-vector has to be synthesized using the surrounding vectors denoted $\overline{V}_x$, $\overline{V}_y$, and $\overline{V}_z$. For example, if $\overline{V}_r$ is located in the fourth region of sector one, we get the following combination: $\overline{V}_x = \overline{V}_1$, $\overline{V}_y = \overline{V}_7$, and $\overline{V}_z = \overline{V}_8$. The application time of each vector depends on the region enclosing the reference vector. Table 1, hereafter provides the appropriate three nearest vectors assuming that $\overline{V}_r$ is located in one of the four regions within the first sector. Table 2 gives the expressions of the duty cycles for the four possible positions of $\overline{V}_r$ within one sector.

The last step is to provide the switching-sequences of the semi-conductors which must take into consideration the following two constraints:

- The number of transitions of each power semiconductor between ON and OFF states must not be superior to two within a switching period.
- The midpoint voltage must remain close to zero.

Table 1. The appropriate nearest three vectors when $\overline{V}_r$ is lying within the four regions of sector 1

	$\overline{V}_x$	$\overline{V}_y$	$\overline{V}_z$
Region 1	$\overline{V}_0$	$\overline{V}_1$	$\overline{V}_2$
Region 2	$\overline{V}_1$	$\overline{V}_8$	$\overline{V}_2$
Region 3	$\overline{V}_2$	$\overline{V}_9$	$\overline{V}_8$
Region 4	$\overline{V}_1$	$\overline{V}_7$	$\overline{V}_8$

Figure 4 illustrates an example of the gates pulses for the upper and the lower transistors of each leg when $\overline{V}_r$ is located in the fourth region of the first sector.

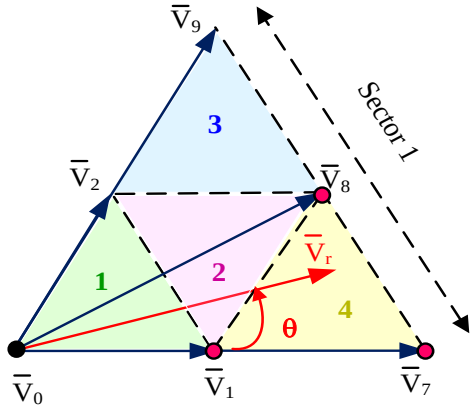

Fig. 3. Triangle identification within sector 1

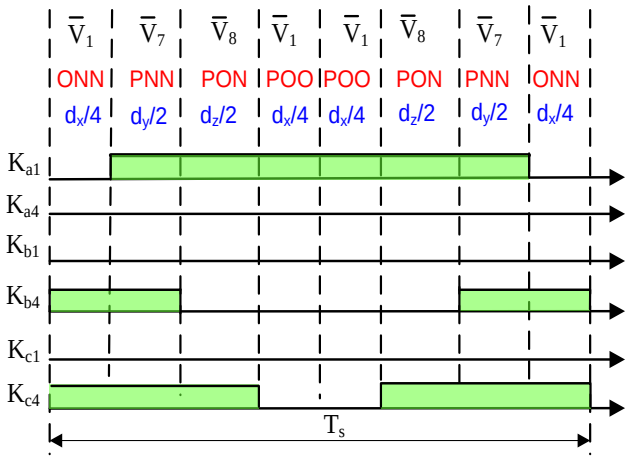

Fig. 4. Switching sequences when $\overline{V}_r$ is located in sector 1, triangle 4

Table 2. Expressions of the duty cycles for the four possible positions of $\bar{V}_r$ within one sector $\left(\rho = 2\sqrt{3}\ \ \frac{|\bar{V}_r|}{V_{dc}}\right)$

	d_x	d_y	d_z
Region 1	$1 - \rho \sin\left(\theta - (K_v - 2)\frac{\pi}{3}\right)$	$\rho \sin\left(K_v\frac{\pi}{3} - \theta\right)$	$\rho \sin\left(\theta - (K_v - 1)\frac{\pi}{3}\right)$
Region 2	$1 - \rho \sin\theta - (K_v - 1)\frac{\pi}{3}$	$-1 + \rho \sin\left(\theta - (K_v - 2)\frac{\pi}{3}\right)$	$1 - \rho \sin\left(K_v\frac{\pi}{3} - \theta\right)$
Region 3	$2 - \rho \sin\left(\theta - (K_v - 2)\frac{\pi}{3}\right)$	$-1 + \rho \sin\left(\theta - (K_v - 1)\frac{\pi}{3}\right)$	$\rho \sin\left(K_v\frac{\pi}{3} - \theta\right)$
Region 4	$2 - \rho \sin\left(\theta - (K_v - 2)\frac{\pi}{3}\right)$	$-1 + \rho \sin\left(K_v\frac{\pi}{3} - \theta\right)$	$\rho \sin\left(\theta - (K_v - 1)\frac{\pi}{3}\right)$

4. The Hexagons' Method

The conventional three-level diagram is decomposed into six small hexagons. Each hexagon can be considered as the space-vector diagram of a 2-level converter that is given by Fig. 5. The position of $\bar{V}_r$ is therefore identified within a singular small hexagon also known as a two-level hexagon. Three fundamental steps are necessary for the implementation of this method: small hexagon identification, duty cycles computation, and switching sequences generation.

Once the appropriate small-hexagon is located (H_1, H_2, ... H_6), the adequate subsector within the selected hexagon must be identified. For this reason, we define a new space vector $\bar{U}_k$ referred to the center of the adequate two-level diagram as shown in Fig. 6. $\bar{U}_k$ can be deduced from the initial reference-vector $\bar{V}_r$ as given in Eq.(3):

$$\bar{U}_k = \bar{V}_r - \frac{V_{dc}}{3} e^{j\left(\frac{H-1}{3}\pi\right)}, \qquad H = (1, \dots 6) \tag{3}$$

With H is the hexagon's number.

Accordingly, the three-level vector diagram can be transformed to an equivalent two-level diagram with $\bar{V}_1$ is the new zero vector which is also referred to as pivot vector; therefore, we can synthesize the new reference voltage vector $\bar{U}_k$ using the same technique applied for two-level voltage source inverters. We should therefore identify the subsector enclosing the new reference vector $\bar{U}_k$, identify the two appropriate adjacent vectors of the small hexagon and compute their application times. For a further explanation, we consider that the $\bar{U}_k$ is situated in the second subsector within hexagon 1 as illustrated in Fig. 6. $\bar{V}_2$ and $\bar{V}_8$ are therefore used as adjacent vectors while $\bar{V}_1$ is referred to as the zero vector. The duty cycles $d_x, d_y, and\ d_0$ that correspond to the relative application times of $\bar{V}_8$, $\bar{V}_2$, and $\bar{V}_1$ are computed as shown in Eq. (4) :

$$\begin{cases} d_x = 2 . \dfrac{\sqrt{3} . |\bar{U}_k| . \sin\left(k_v \frac{\pi}{3} - \theta\right)}{V_{dc}} \\ d_y = 2 . \dfrac{\sqrt{3} . |\bar{U}_k| . \sin\left(\theta - (k_v - 1)\frac{\pi}{3}\right)}{V_{dc}} \\ d_0 = 1 - d_x - d_y \end{cases} \tag{4}$$

"θ": The phase-angle of the new reference-vector $\bar{U}_k$.

"k_v": The subsector number of the small-hexagon.

The last step provides the adequate switching states at each sampling period. Similar to the previous approach, the constraints concerning the number of ON/OFF switching and the mid-point dc-bus voltage balance must be respected. Figure 7 shows an example of the switching sequences distribution which correspond to a reference-vector located in the first hexagon and the second subsector.

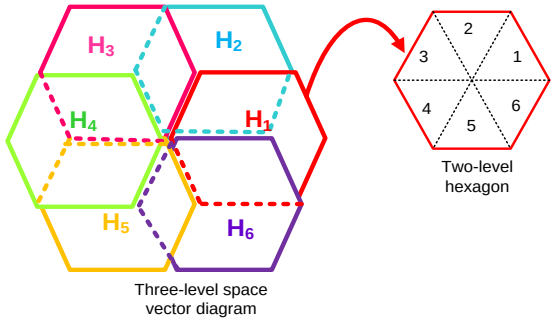

Fig. 5. 3–level space-vector diagram decomposed into 6-small hexagons

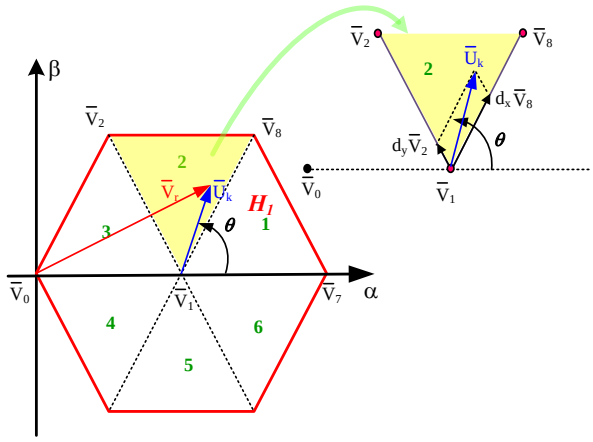

Fig. 6. New reference vector determination and synthesis

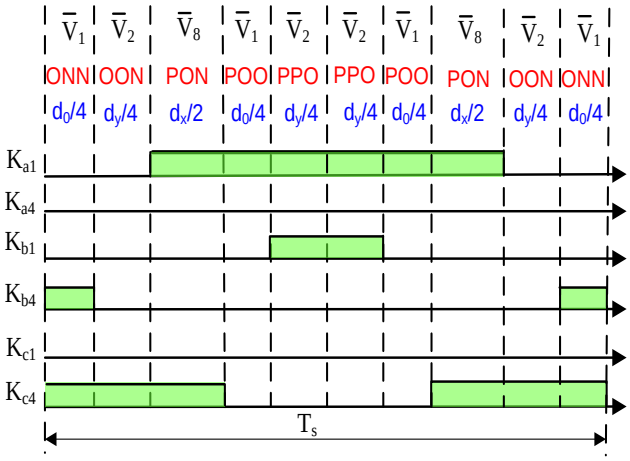

Fig. 7. Switching-pattern distribution

5. Simulation Results and Comparison

A numerical model of a 3-level NPC dc-ac converter feeding a star connected R-L load is implemented using Matlab/Simulink software. Table 3 gives the electrical system and control algorithm parameters.

First, all the simulation waveforms of the NTV method are provided in Fig. 8 with the modulation index m = 1.15. Figure 8a shows the modulated pole-voltages with reference to the mid-point of the dc-bus, V_{ao} which draws three levels. The output voltage V_{ab} is presented in Fig. 8b where the number of levels is equal to 5. Figure 8c illustrates the phase-to-neutral modulated voltage waveform which has a quasi-sinusoidal shape. Figure 8d shows the high quality of the load currents waveforms which are quite sinusoidal and balanced.

Figures 8e-f display the voltages across the upper and the lower dc-bus capacitors, V_{Po} and V_{oN}. One can observe that these latter are almost equal to $V_{dc}/2$; this implies that the SVPWM technique and switching strategy are apt to balance the voltage across the capacitors in case of balanced load. A second test is performed to validate the proper operation of the hexagon method, when m = 0.8. The obtained results are illustrated in Fig. 9. Figures 9a-b show that the load currents draw also quite sinusoidal and balanced waveforms while the phase-to-neutral modulated output voltage draws a quasi-sinusoidal shape.

The comparative analysis is primarily carried out in terms of output voltages and load currents THDs. Figures 10a-b-c display the variation in THD of the modulated output voltage V_{ab}, the filtered output voltage and the load current respectively, with respect to the modulation index m. As it is observed in Fig. 10a, both modulation methods provide the same THD of the modulated output voltage V_{ab}. However, after applying a low-pass filter, the THD obtained with the NTV method becomes much lower than the one obtained with the hexagon method for m varying from 0.2 to 0.8. This means that the NTV method provides harmonic components with lower amplitude in the low-frequency range. On the other hand, for m superior or equal to 0.8, the obtained THDs remain similar for both modulation methods. This result is emphasized by inspecting Fig.10c, which shows effectively that the NTV method provides a better THD of the load current when m is varying from 0.2 to 0.8.

Table 3. Simulation parameters

Parameter description	Value
Load resistance	R = 20.5 Ω
Load inductance	L = 10 mH
Dc-bus voltage	V_{dc}=100 V
Dc-bus capacitor	C_{dc}= 940 µF
Switching and sampling frequencies	Fc = 5 kHz
Output frequency	f_o = 50 Hz.

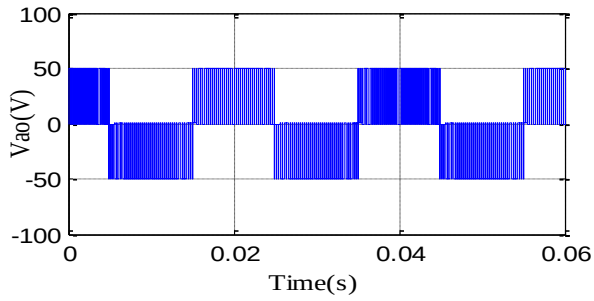

(a)

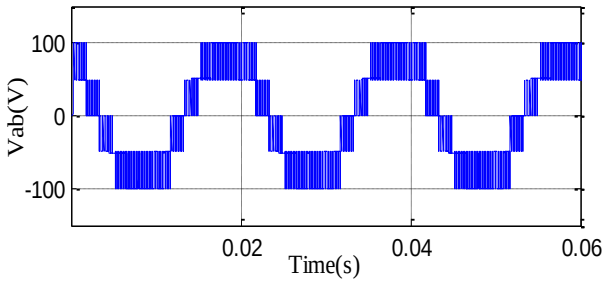

(b)

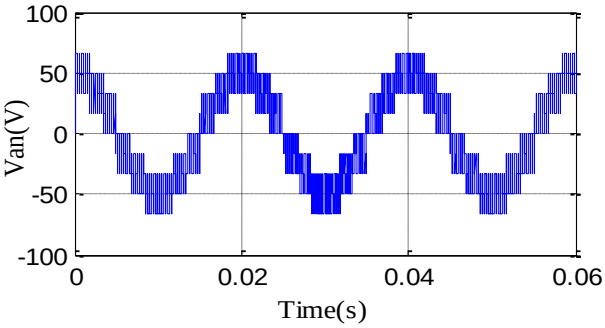

(c)

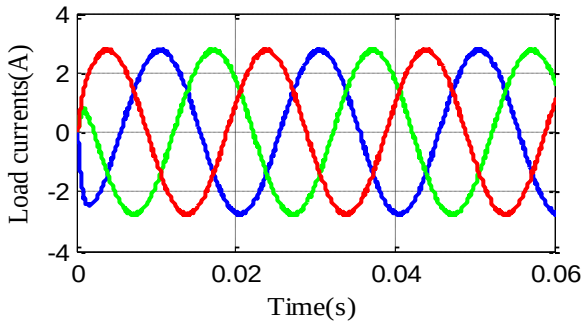

(d)

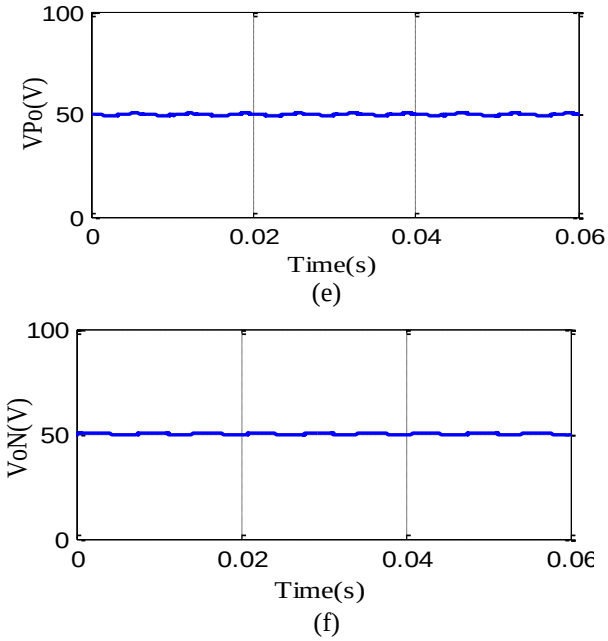

Fig. 8. Simulation results obtained with the NTV method for m=1.15 (a) pole-voltage V_{ao}, (b) line-to-line voltage V_{ab},(c) phase to neutral voltage V_{an} ,(d) load currents,(e) and (f) upper and lower voltages across the dc-link capacitors V_{Po} and V_{oN}

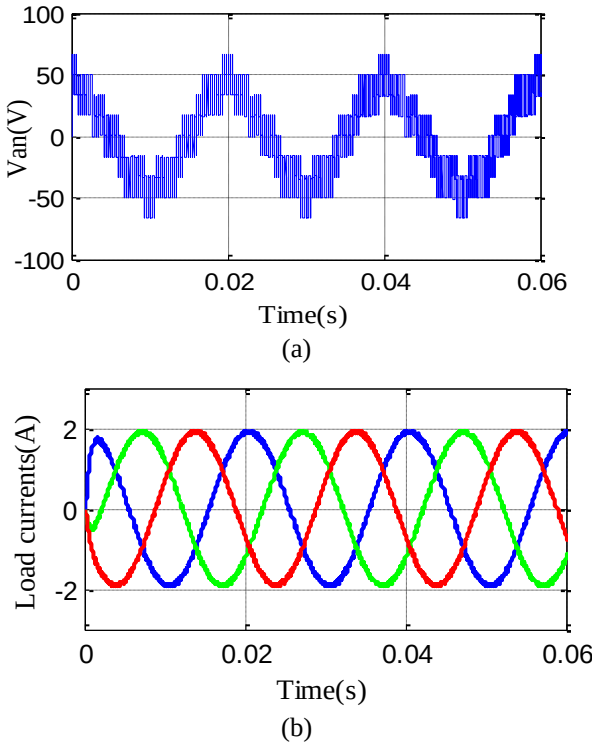

Fig 9. Simulation results obtained with the hexagon method for m=0.8, (a) phase-to-neutral voltage V_{an}, (b) load currents

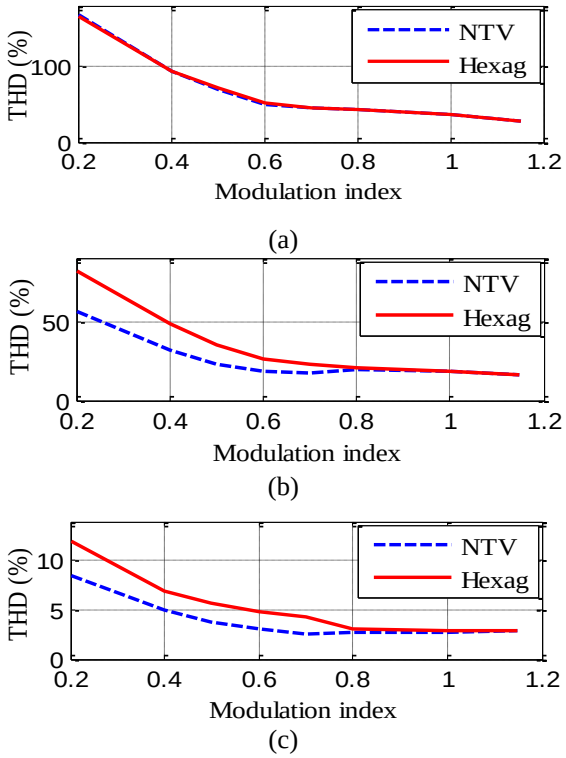

Fig. 10. THD of (a) Modulated output voltage V_{ab}, (b) Filtered voltage V_{ab}, (c) Load-current versus m variation

The comparative study is also carried out in terms of an important performance criterion namely the common mode voltage ($V_{CM} = V_{no}$). Note that this voltage affects the leakage current flowing through the load to the ground, which leads to an electromagnetic interference (EMI). Figure 11a displays the common mode voltage waveforms obtained with the two modulation methods and m = 0.4. For this operation point, V_{CM} obtained with the hexagon method is varying within the range $[-V_{dc}/3, V_{dc}/3]$, while for the case of the NTV method, it varies between $-V_{dc}/2$ and $+V_{dc}/2$. To better quantify the performance in terms of common mode voltage, we computed the frequency spectra that are displayed in Fig.12a. One can observe that the amplitudes of the low-frequency components are larger with the hexagon method though in time domain we observed that the variation range of V_{CM} is less important than the NTV method. In the high frequency range, the two methods provide approximately the same performance. Indeed, the NTV method provides more important peaks at 15 kHz, 20 kHz, 40 kHz, and 70 kHz while the hexagon method generates higher peaks at 10 kHz, 25 kHz, 45 kHz, and 65 kHz. Figure 12b displays the frequency spectra obtained with m = 0.6. For this operation point, the hexagon method provides harmonic components with larger amplitudes especially at 5 kHz and 20 kHz and also at low frequencies. The same remarks remain valid for m = 0.8 as illustrated in Fig.12c. However, the difference between both methods is less important than the case when m = 0.6. On the other hand, Figs.11b and 12d display the time-domain waveforms and frequency spectrum of V_{CM} obtained with m = 1.15. It is clear that both modulation methods provide the same common mode voltage with this maximum modulation index value.

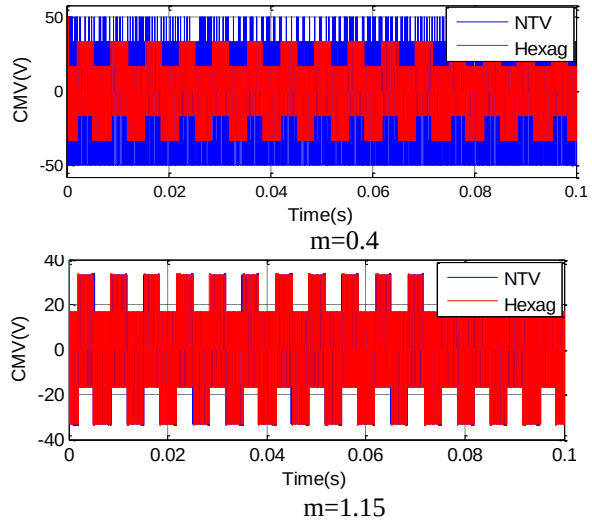

Fig. 11. Common mode voltages obtained with both methods for two different values of m

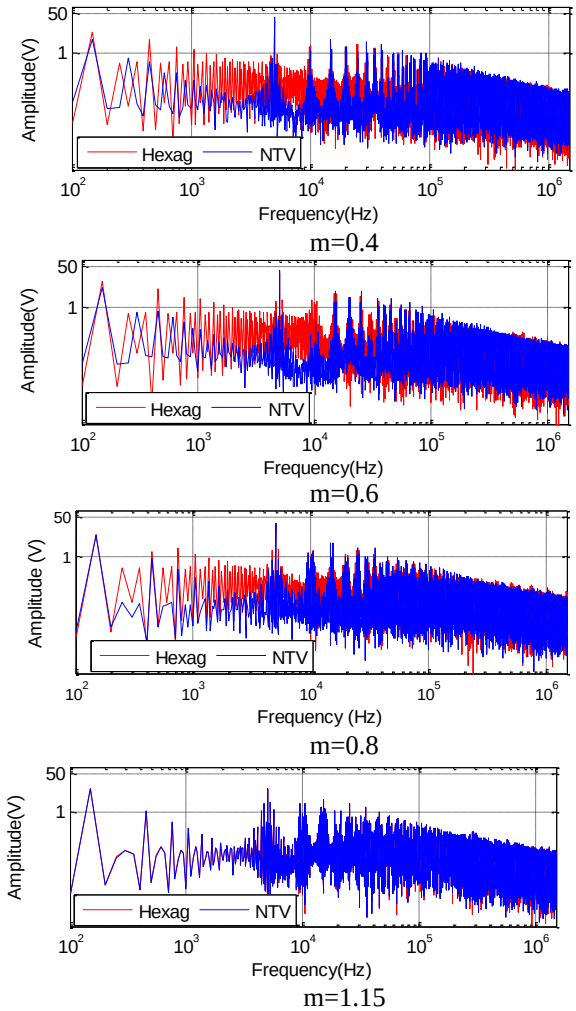

Fig. 12. Frequency spectra of the common mode voltages obtained with numerical simulations for different values of the modulation index

6. Experimental Results

Aiming to confirm the comparative study results based on simulation tools, a scaled down prototype of a 3-level NPC converter is built using the IREF 740 MOSFET transistors and 15ETH06 clamping diodes. Both algorithms are implemented in real-time on the DSP TMS320F28335 from Texas Instruments operating at 150 MHz. The control signals are routed from the DSP output peripherals to the transistors gates through the opto-drivers HCPL 3120. A photo of the experimental setup is given by Fig. 13. The same parameters used in simulation are adopted to perform the real-time implementation.

The first experiment is realized using the NTV method with a maximum modulation index m =1.15. Figure 14 displays the line-to-line output voltages, load currents waveforms, the lower and the upper voltages across the dc-bus, and the common mode voltage V_{no}. It is clear that the obtained experimental waveforms are quite similar to those obtained with simulations. An additional high frequency ripple is observed in the output current waveform; it is mainly caused by the switching operation and stray inductance as well as the parasitic capacitance of the power circuit.

Figure 15 displays the modulated output voltage (V_{ab}) and load current THDs. The experimental results perfectly match those obtained with simulations and clearly prove that the NTV technique provides a better quality of the load currents for low values of the modulation index m. Figure 16 displays the frequency spectra of the common mode voltage experimental waveforms which are similar to those achieved with numerical simulations. Indeed, the hexagon method provides harmonic components with larger amplitude in the low-frequency range for m = 0.4, 0.6 and 0.8. For m = 0.6, the amplitude of the spectral ray obtained with the hexagon method and located at 10 kHz is much more important than those obtained with the NTV method. Finally, we can notice that both methods provide quite similar results with the maximum value of m = 1.15.

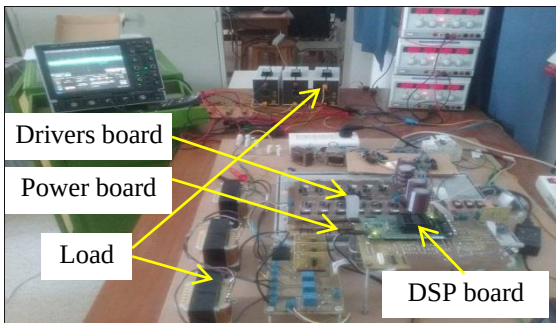

Fig. 13. Photo of the experimental setup

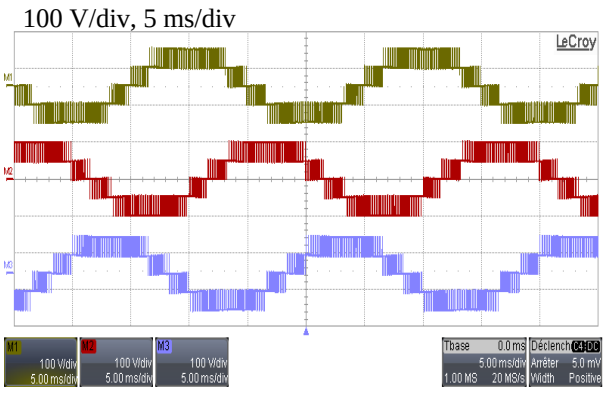

(a)

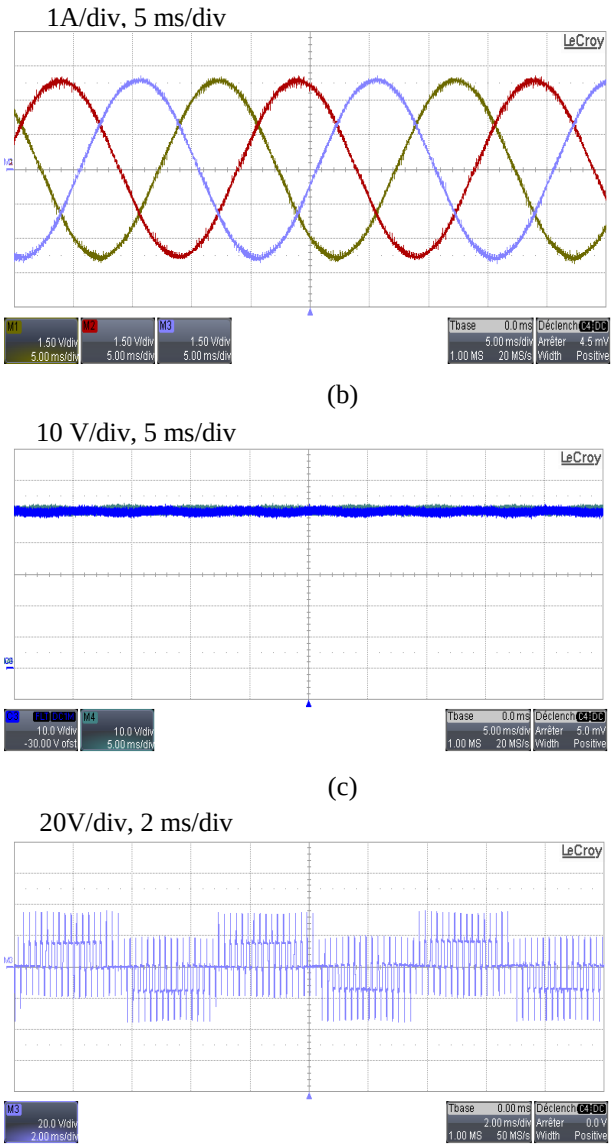

Fig. 14. (a) Line-to-line output voltages, (b) load currents, (c) V_{Po} and V_{oN} voltages,(d) common mode voltage V_{no}, obtained with the NTV method and m = 1.15

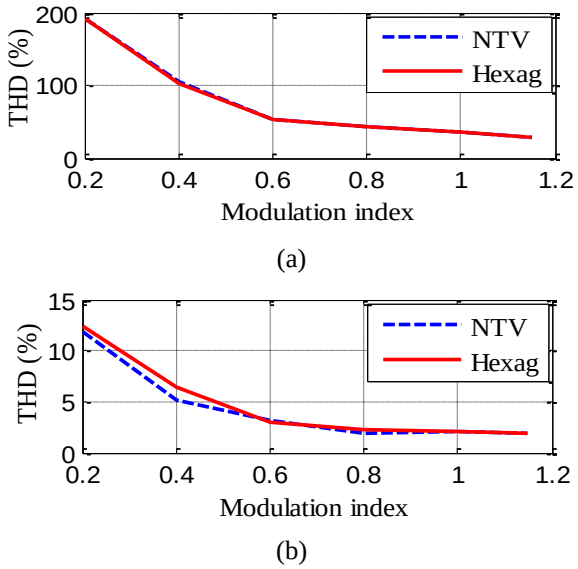

Fig. 15. THD of (a) line-to-line modulated output voltage V_{ab}, (b) Load currents versus the modulation index

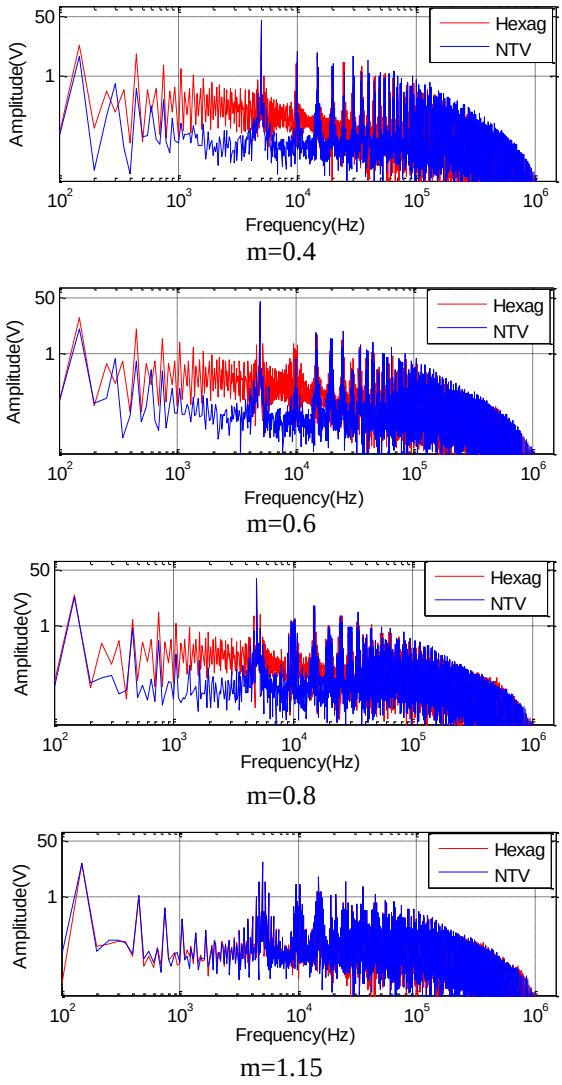

Fig. 16. Frequency spectra of the common mode voltages obtained with experimental results and for different values of m

The comparative analysis is also carried out in terms of the Electromagnetic Interference EMI since it represents, nowadays, a very important criterion adopted by several standards for the evaluation of the disturbance generated by a PWM converter [27]. For this purpose a line impedance stabilizing network (LISN) is inserted between the dc-source and the dc-bus terminals as shown in Fig. 17. Firstly, the voltages V_{R1} and V_{R2} across the two LISN resistors are measured using a 10 GS scope. Figure 18 provides an example of voltages waveforms across the LISN resistors. The obtained results are saved as data format and next loaded in the Matlab workspace. The common mode and differential mode emissions are therefore deduced from V_{R1} and V_{R2} as demonstrated in Eqs. (7) and (8) hereafter:

$$V_{CM} = \frac{V_{R1} + V_{R2}}{2} \tag{7}$$

$$V_{DM} = \frac{V_{R1} - V_{R2}}{2} \tag{8}$$

Finally, the time domain waveforms of V_{CM} and V_{DM} are transferred into the frequency domain using the FFT tool. Figure 19 displays the frequency spectra of the conducted emissions (common mode and differential mode) obtained with both modulation algorithms for m = 1.15. Figure 20 displays the frequency spectra of the common mode emission obtained with

both modulation algorithms under the variation of m. The frequency range is set between 150 kHz and 30 MHz. For m = 0.2, 0.4, 0.8, and 1, both methods provide almost the same common mode emission. However, for m = 1.15 and m = 0.6, one can observe that the hexagon method provides more conducted emissions than the NTV. For m = 1.15, the difference is observed in the amplitude of the spectral ray located at 1.1 MHz which exceeds 72 dBµV. For m = 0.6, the difference is observed at two spectral rays located at 1.1 MHz and 300 kHz respectively. As for the differential mode emission, one can observe that both methods provide approximately the same performance with m = 1.15.

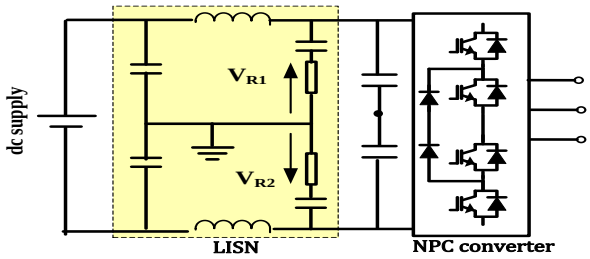

Fig. 17. Electrical circuit of the LISN used to measure the conducted emissions

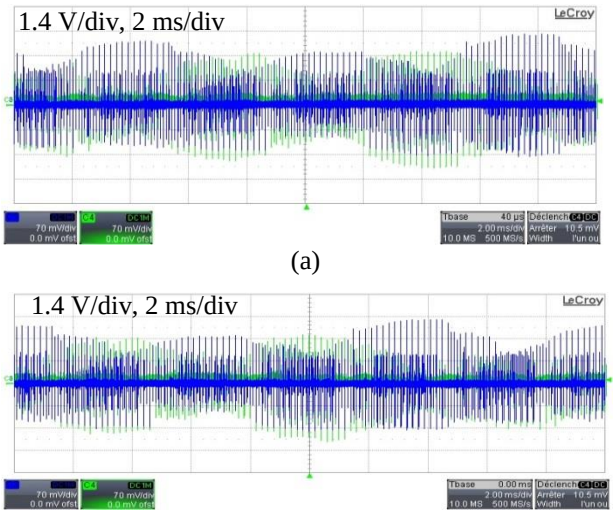

Fig. 18. Voltages waveforms V_{R1} (blue) and V_{R2} (green) across the two LISN resistors obtained with m =1.15 (a) NTV method, (b) hexagon method

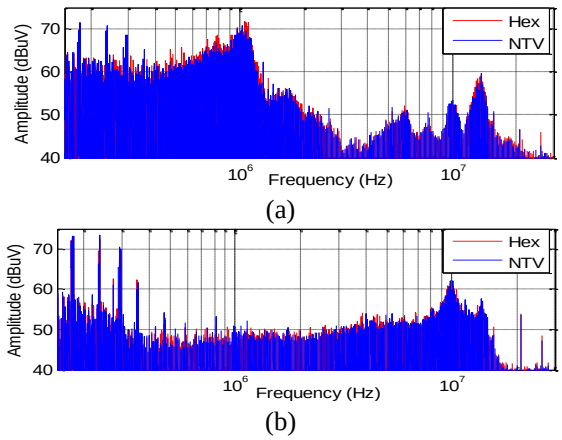

Fig. 19. Frequency spectra of the conducted emission obtained with m = 1.15 (a) common mode emission, (b) differential mode emission

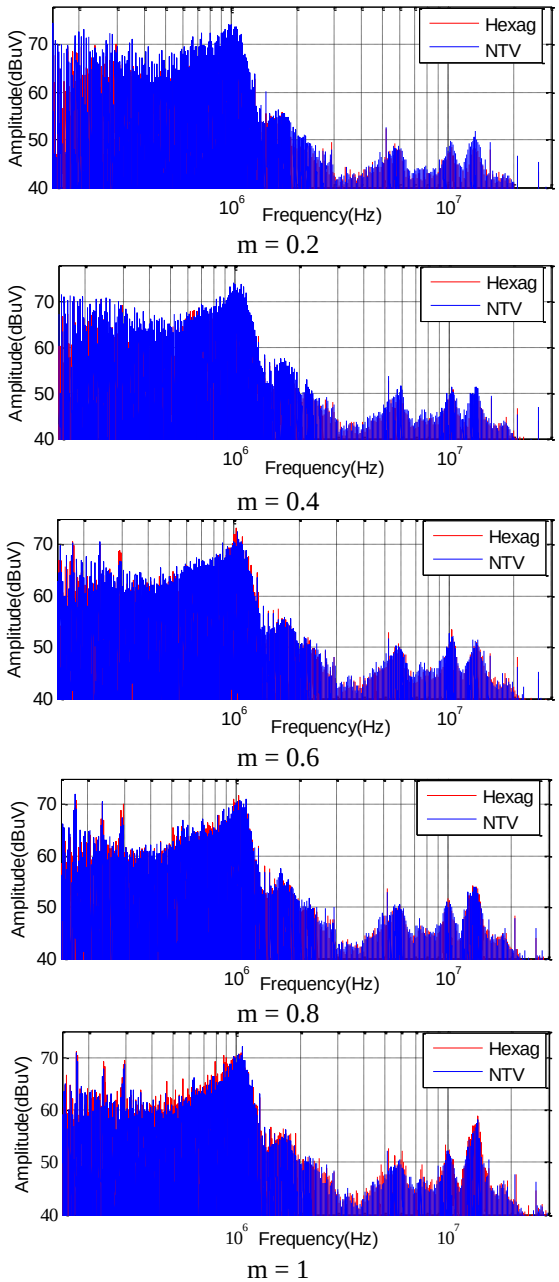

Fig. 20. Frequency spectra of the common mode emission obtained under the variation of m

Finally, in Fig. 21, the inverter's efficiency is displayed with respect to the modulation index variation. When m is lower than 0.4, the efficiency obtained with the hexagon method is a little bit better than the one obtained with the NTV method. However, for m = 0.6, the efficiency becomes much more important with the NTV method. Finally, for "m" superior or equal to 0.8, one can observe that the inverter's efficiency remains the same for both modulation methods.

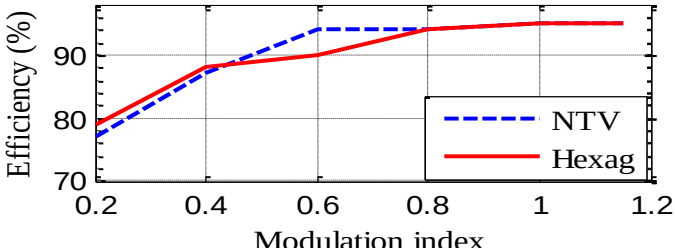

Fig. 21. Efficiency as a function of the modulation index

7. Conclusion

This paper performed a detailed comparative study between two SVPWM strategies: the NTV method and the hexagon method. The comparison is carried out in terms of THD, CMV, conducted emissions and efficiency criteria. The following conclusions and remarks are recorded:

- THD: the numerical and experimental results show that the NTV approach presents the best performance under low values of m. However, the obtained THDs remain similar for both modulation methods when m is superior or equal to 0.8.

- CMV: the hexagon method provides harmonic components with larger amplitude for m = 0.4, 0.6 and 0.8. However, for m = 1.15, both methods have similar performance in terms of CMV.

- Conducted emissions: the study showed that both methods provide almost the same common mode emission for the low values of m. However, for m = 1.15, the hexagon method provides higher conducted emissions than the NTV method. Note that, both methods have the same performance in terms of differential mode emission for m = 1.15.

- Efficiency: the hexagon method has a better efficiency than the one achieved with the NTV method when m is lower than 0.4. However, the efficiency is more important with the NTV method for m = 0.6. It remains the same for both modulation methods when m is superior or equal to 0.8.

References

[1] K.K. Gupta, A. Ranjan, P. Bhatnagar, L. Kumar Sahu, S. Jain, "Multilevel Inverter Topologies With Reduced Device Count: A Review", *IEEE Trans. Power Electron.*, vol.31, no.1, pp.135 – 151, Jan.2016.

[2] Y. Soufi, S. Ghoudelbourk, T. Bahi, H. Merabet, "Harmonics Minimization of Multilevel Inverter Connecting Source Renewable Energy", *International Journal Of Renewable Energy Research, IJRER* vol.1, no.4, pp.265-270 ,2011.

[3] F. A. Gervasio, E. Bueno, R. A. Mastromauro, M. Liserre and S. Stasi, "Voltage control of microgrid systems based on 3lnpc inverters with LCL-filter in islanding operation," *2015 International Conference on Renewable Energy Research and Applications (ICRERA*), Palermo, 2015, pp. 827-832.

[4] I. Moussa, A. Bouallegue, A. Khedher, "3 kW Wind Turbine Emulator Implementation on FPGA Using Matlab/Simulink", *International Journal of Renewable Energy Research*, vol.5, no.4, pp.1155-1163, 2015.

[5] E. Mahersi, A. Khedher, M.F. Mimouni, "The Wind energy Conversion System Using PMSG Controlled by Vector Control and SMC Strategies", *International Journal of Renewable Energy Research*, vol.3, no.1, pp.42-50, 2013.

[6] S.Amara, A. Bouallegue, A. Khedher, "Theoretical and Practical Study of a Photovoltaic MPPT Algorithm Applied to Voltage Battery Regulation", *International Journal of Renewable Energy Research*, vol.4, no.1, pp.84-90, 2014.

[7] S. Pugliese, R. A. Mastromauro and S. Stasi, "Simplified feedback linearization control of a single-phase photovoltaic NPC converter in direct-quadrature rotating reference frame," *2015 International Conference on Renewable Energy Research and Applications (ICRERA)*, Palermo, 2015, pp. 1369-1375.

[8] I. Vechiu, A. Etxeberria, H. Camblong and Q. Tabart, "Control of a microgrid-connected hybrid energy storage system," *2014 International Conference on Renewable Energy Research and Application (ICRERA)*, Milwaukee, WI, 2014, pp. 412-417.

[9] F.Z. Lahouar, M. Hamouda, J. Ben Hadj Slama, F. Ben Mustapha, " Comparative Study between Two and Three-level topologies of Grid- Connected Photovoltaic Converters", *In: International Renewable Energy Congress (IREC 2014)*,March 2014.

[10] J. H. Seo, C.H. Choi, D.S. Hyun, "A new simplified space-vector PWM method for three-level inverters", *IEEE Trans. Power Electron*., vol. 16, no. 4, pp. 545–550, July 2001.

[11] I.O. Charles, "A Cascaded Multi-level Inverter Topology with Improved Modulation Scheme", *Electric Power Components and Systems*, vol.42, no.7, pp.768–777, 2014.

[12] S. Benanti et al., "Experimental analysis with FPGA controller-based of MC PWM techniques for three-phase five level cascaded H-bridge for PV applications," *2016 IEEE International Conference on Renewable Energy Research and Applications (ICRERA)*, Birmingham, 2016, pp. 1173-1178.

[13] J. Rodriguez, J. S. Lai, and F. Z. Peng, "Multilevel inverters: A survey of topologies, controls, and applications," *IEEE Trans. Ind. Electron.*, vol. 49, no. 4, pp. 724–738, Aug. 2002.

[14] R. Geetha, M. Ramaswamy, "New PWM strategy for three-phase multilevel inverter", *Int. J. Power Electronics*, vol. 7, no. 1/2, pp.86–108, 2015.

[15] M. Rajesh, B. Singh, "Three-level NPC rectifier-based midpoint converter-fed SRM drive", *Int. J. Power Electronics*, vol. 6, no. 1, pp.1–17, 2014.

[16] B. Mwinyiwiwa, Z. Wolanski, B.T. Ooi, "Microprocessor implemented SPWM for multi-converters with phase-shifted triangle carriers", *IEEE Trans. Ind. Appl.* ,vol. 34, no. 3, pp. 487- 494, May/June 1998.

[17] V. Oleschuk, V. Ermuratskii and F. Blaabjerg, "Six-phase vehicular drive with renewable dc sources and hybrid PWM control of four inverters," *2015 International Conference on Renewable Energy Research and Applications (ICRERA)*, Palermo, 2015, pp. 515-519.

[18] C. Bharatiraja, J. L. Munda, R. Bayindir and M. Tariq, "A common-mode leakage current mitigation for PV-grid connected three-phase three-level transformerless T-type-NPC-MLI," *2016 IEEE International Conference on Renewable Energy Research and Applications (ICRERA)*, Birmingham, 2016, pp. 578-583.

[19] W.A. Hill, C.D. Harbourt, "Performance of medium voltage multi-level inverters", *Thirty-Fourth IAS Annual Meeting. Conference Record of the 1999 IEEE*, Phoenix, AZ, vol.2, pp.1186 – 1192, 03-07 Oct. 1999.

[20] S. Wei, B. Wu, F. Li, C. Liu, "A general space vector PWM control algorithm for multilevel inverters", *in Proc. 18th Annual. IEEE APEC*, vol. 1, pp. 562–568, February 2003.

[21] D.C Lee, G.M Lee, "A novel over modulation techniques for space vector PWM inverters", *IEEE Trans. Power Electron.*, vol.13, no.4, pp.953-963, Oct 1993.

[22] S. Maryam , S.R. Hamidreza, B. Alireza,I. Reza, "A Neuro-Based Classification Algorithm for Implementation of Space Vector Modulation for Multi-Level Converters", *EPE Journal*, vol.18,no.2,pp.41-49, 2008.

[23] F.Z. Lahouar, S. Kraiem, M. Hamouda, J. Ben Hadj Slama, "DSP based real-time implementation of a space vector modulation scheme for three-phase three-level NPC converter", *International Renewable Energy Congress (IREC 2015),* March 2015.

[24] M. Hamdi, M. Hamouda, F. Fnaiech, and K. AI-Haddad, "Space vector pulse width modulation of multilevel inverters: A new method for selecting the appropriate small hexagon", *38th Annual Conference on IEEE Industrial Electronics Society (IECON 2012)*, Montreal, QC, Canada, pp. 774 – 779, 25-28 Oct. 2012.

[25] N. Celanovic, D. Boroyevich, "A fast space vector modulation algorithm for multilevel three phase converters", *IEEE Trans. Indus. Appl.*, vol.37, no.2, pp. 637–41, Mar/Apr 2001.

[26] L. Li-Suel, K. Nam-Joon, H. Dong-Seok, "A Simplified Space-Vector PWM Scheme for N-Level NPC Inverter Based on Two-Level Space-Vector PWM", *Vehicle Power and Propulsion Conference (VPPC)* , pp.1-6, 2014.

[27] Dj. Lalili, N. Lourci, E. M. Berkouk, F. Boudjema, J. Petzoldt , and M. Yasin Dali, "A Simplified Space Vector Pulse Width Modulation Algorithm For Five Level Diode Clamping Inverter", *in the International Symposium on Power Electronics, Electrical Drives, Automation and Motion, SPEEDAM 2006*, Taormina, pp. 1349 – 1354,23-26 May 2006.

[28] E. Prasad, A. Sudhakar, V. Kumar, "Simulation of five-level inverter fed PMSM based on fast SVPWM", *IEEE International Conference on Power Electronics, Drives and Energy Systems, PEDES 2012*, Bengaluru, pp. 1-5,16-19 Dec. 2012.

[29] M.C. Cavalcanti, A.M. Farias, K.C. Oliveira, F.A.S. eves, J.L. Afonso, "Eliminating Leakage Currents in Neutral Point Clamped Inverters for Photovoltaic Systems", *IEEE Trans. Ind. Electron.*, vol.59 , no.1, pp.435 – 443, Jan.2012.

[30] A. Choudhury, P. Pillay, S. Williamson, "Comparative Analysis Between Two-Level and Three-Level DC/AC Electric Vehicle Traction Inverters Using a Novel DC-Link Voltage Balancing Algorithm", *EEE J. Emerg. Sel. Top. Power Electron.* vol.2, no.3, pp. 529 – 540, Sept. 2014.

[31] M. Valan Rajkumar, P.S. Manoharan, A. Ravi, "Simulation and an experimental investigation of SVPWM technique on a multilevel voltage source inverter for photovoltaic systems", *Electrical Power and Energy Systems*, vol. 52, pp. 116–131, 2013.

[32] P. Muhamed Shereef, G. Shiny, "A Simplified Space Vector PWM Scheme for any N-Level Inverter", *IEEE Students' Technology Symposium (TechSym),* Kharagpur, pp. 176 – 181, Feb. 28 2014-Mar. 2014.

[33] M. Salem, M. Hamouda, J. Ben Hadj Slama, "Comparative study of conventional modulation schemes in terms of conducted and radiated emi generated by three-phase inverters", Turk J ElectrEng Co., doi: 10.3906/elk-1508-61.